HHS Public Access

Author manuscript

Handb Clin Neurol. Author manuscript; available in PMC 2015 June 26.

Published in final edited form as:

Handb Clin Neurol. 2012 ; 109: 85–101. doi:10.1016/B978-0-444-52137-8.00006-1.

Advanced MRI Strategies for Assessing Spinal Cord Injury

Seth A. Smith, Ph.D.,

Vanderbilt University Institute of Imaging Science, Department of Radiology and Radiological Sciences, Department of Biomedical Engineering, 1161 21st Ave South, MCN AAA3111, Nashville, TN 37232

James J. Pekar, Ph.D., and

F.M. Kirby Research Center for Functional Brain Imaging, Russell H. Morgan Department of Radiology and Radiological Sciences, 707 N. Broadway, Baltimore, MD 21205

Peter C.M. van Zijl, Ph.D.

F.M. Kirby Research Center for Functional Brain Imaging, Russell H. Morgan Department of Radiology and Radiological Sciences, 707 N. Broadway, Baltimore, MD 21205

Introduction

The ability of magnetic resonance imaging to non-invasively characterize properties of living tissue has made MRI a celebrated hallmark of modern medicine and widely used for the diagnosis and prognosis of many clinical conditions. MRI is flexible; the magnetic resonance signal can be sensitized to various properties by using different schemes for the excitation, encoding, and detection of nuclear magnetization. Among the simplest of these many contrast mechanisms are the exponential decay of the detectable transverse magnetization (characterized by the transverse relaxation time, T_2) and the exponential recovery of the longitudinal magnetization (characterized by the longitudinal relaxation time, T_1). T_1- and T_2-weighted MRI have served to identify and follow lesions in diseases such as, but not limited to, cancer (Bydder and Steiner 1982; Huk and Heindel 1983) and multiple sclerosis (Grossman et al. 1986; Scotti et al. 1986), and to follow the clinical course of disorders including dementia (Bastos Leite, Scheltens, and Barkhof 2004; Rodrigo et al. 2004), stroke (Moseley, Wendland, and Kucharczyk 1991; Sevick et al. 1990), and Alzheimers disease (Bastos Leite, Scheltens, and Barkhof 2004; Rodrigo et al. 2004). In the 1990's, alternative MRI contrast mechanisms, including magnetization transfer (MT) and diffusion tensor imaging (DTI) were developed. These methods sought to probe the tissue at its microscopic level by using magnetic resonance to report upon the tissue's macromolecular composition (using MT-MRI) or the directional anisotropy of water's Brownian motion induced by axonal anatomy (with DTI).

Over the past two decades, methods such as MT (Wolff and Balaban 1989), DTI (Basser, Mattiello, and LeBihan 1994; Melhem et al. 2002), quantitative T_2 (MacKay et al. 1994; Whittall et al. 1997), q-space/q-ball (Cohen-Adad et al. 2008; Hagmann et al. 2006; Wu and Alexander 2007), high angular resolution diffusion imaging (HARDI) (Tuch 2004),

Corresponding Author: Peter C.M. van Zijl, Ph.D.

perfusion mapping using arterial spin labeling (CBF/ASL) (Deibler et al. 2008, 2008, 2008), functional MRI (fMRI), and magnetic resonance spectroscopy (MRS) and spectroscopic imaging (MRSI) have been widely applied to the brain. However, application of these more advanced methods to the spinal cord has been limited, because of challenges such as smaller size, motion of the cord induced by cerebrospinal fluid (CSF) pulsations within the spinal canal.

In spite of major progress towards routine use of advanced MRI strategies in the brain, technical developments in the spinal cord have been slow. To date, the bulk of spinal cord imaging is still performed using conventional imaging sequences. In particular, T_1-weighted imaging has been used to assess the prevalence of active lesions for diseases such as multiple sclerosis (MS). New inflammatory lesions that have caused a breakdown in the blood-brain/spinal cord barrier show pronounced image signal enhancement after administration of gadolinium contrast agents, as well as chronic hypo-intensity, the so-called T_1 black holes (Scotti et al. 1986). Fluid attenuated inversion recovery (FLAIR) (Hajnal et al. 1992; White et al. 1992) imaging has been utilized to highlight inflammation (De Coene et al. 1992) by nulling the signal arising from CSF. T_2-weighted imaging, as a counterpart to FLAIR, has also been used to identify lesions in the cord; and T_2-based assessments of the volume and number of these lesions have been shown to relate to neurological deficits. When disc disease is suspected, methods such as the balanced gradient echo, or steady state free-procession (SSFP) are used to achieve useful contrast between spinal cord tissue and surrounding CSF, and between soft tissue surrounding the spinal canal and the canal itself.

Why are the more advanced quantitative MRI methods (e.g., MT-MRI & DTI) not yet routinely employed for spinal cord examinations? The primary reason is size. The spinal cord is small, at most 1.5 cm in cross-section at the cervical and throaco-lumbar bulge. MRI is a relatively insensitive technique that requires relatively large image volume elements (voxels) to generate sufficient imaging signal to noise (SNR). MT and DTI methods use only a fraction of the total available nuclear magnetization, and therefore require either larger voxels or longer acquisition times. For example, DTI in the brain generally requires a spatial resolution on the order of 2 – 3 mm, which is too coarse for the spinal cord. The higher spatial resolution needed for this smaller structure can be achieved, but only with longer acquisitions, leading to increased susceptibility to motion-induced artifacts and image degradation.

Another obstacle to MRI of the cord is that many advanced brain imaging studies use echo planar imaging (EPI) image encoding (Mansfield 1984) to greatly decrease acquisition times. However, EPI image quality suffers in structures that are proximal to tissue interfaces, such as areas near the sinuses, or in the case of the spinal cord, near the surrounding vertebrae. EPI is very sensitive to magnetic field inhomogeneities and such regions often exhibit heavily distorted images that are difficult to interpret.

If such technical barriers can be overcome, application of advanced, quantitative imaging methods to the spinal cord should be rewarding. The spinal cord is somatotopically organized, with a relatively simple structure having 3 major white matter (WM) subdivisions and one internal gray matter (GM) boundary: two lateral columns, two dorsal columns, and

two ventral columns. Thus, quantitative imaging with spatial resolution adequate to resolve these substructures should yield information that can be compared with the neurological function of each of the spinal cord tracts.

The goal of this chapter is to critically review the more advanced, quantitative MRI contrasts that can be obtained to study neurological damage to the spinal cord. We will focus on methods targeted at 1) the composition, orientation, and organization of macromolecules; 2) metabolic and functional activities; and 3) spinal cords in which metal hardware has been implanted following traumatic injury. In section 1, we review methods that probe myelin and axonal constituents, namely MT-MRI, DTI, q-space imaging, and myelin water T_2-based imaging. In section 2, we examine recent advances in the application of MR spectroscopy and functional MRI (fMRI) to the spinal cord. Finally, since one of the hallmarks of traumatic spinal cord injury is the placement of stabilization hardware, section 3 will explore very recent advances in MRI of the spinal cord in situations where metal can be a confounding factor.

Section 1: Assessment of macromolecular composition, tissue orientation and organization

1.1 Magnetization Transfer MRI

Background—Magnetization Transfer (MT) is a general term describing the exchange of magnetization between two nuclei. More specifically, MT studies *in vivo* relate to the magnetic interaction between protons existing in two disparate milieus. In the case of the central nervous system, the protons in, or intimately associated with, macromolecules (so-called semi-solid protons) exchange information with the protons of the surrounding bulk water (Henkelman, Stanisz, and Graham 2001; Wolff and Balaban 1989). While such exchange is a constantly occurring phenomenon, an MT experiment allows specific observation of this exchange process, thereby allowing for indirect assessment of the macromolecular protons via the more abundant and detectable MR signal from the bulk water. A direct measurement of semi-solid protons cannot be made with conventional (T_1- or T_2-weighted) MRI methods due their short transverse relaxation times (on the order of μs) compared to the relaxation time of conventionally observed protons (~tens to many hundreds of ms, depending on the magnetic field strength used). While conventional MRI methods can indirectly reveal pathology related to changes in water content (e.g., edema and inflammation), MT-MRI reports on the semi-solid tissue component, opening the door to assessing macromolecular pathologies such as demyelination (Schmierer et al. 2004).

A conventional MT experiment consists of applying radiofrequency (RF) irradiation of a particular power at a non-specific frequency off-resonance with respect to water, which results in a water signal attenuation. Off-resonance irradiation can be used because the short T_2 of the semi-solid protons gives rise to a very broad MR lineshape (Bryant 1996) that can be as much as 100× the width of the main water resonance. When off-resonance RF irradiation is applied in tissues with semi-solid components, the obtained image shows a reduction in signal (dependent on the irradiation power, bandwidth, and offset of irradiation as well as the tissue T_1) when compared to the same image taken in the absence of

irradiation. The size of the MT effect is sensitive to tissue composition, e.g. degree of myelination. In particular, WM exhibits a greater MT effect than gray matter (GM), which in turn shows greater MT than cerebrospinal fluid (CSF)

The MT effect in white matter has been hypothesized to reflect myelination (Catalaa et al. 2000; Dousset et al. 1992; Filippi and Rocca 2004; Gass et al. 1994; Harrison, Bronskill, and Henkelman 1995; Henkelman, Stanisz, and Graham 2001; Morrison and Henkelman 1995; Ropele et al. 2003; Stanisz et al. 1999; Tortorella et al. 2000; Wolff and Balaban 1989; Yarnykh 2002) since the major constituent of white matter is myelin. However, the MT phenomena cannot discriminate the origins of the exchanged saturation, and current literature only hints at the ability of MT MRI to distinguish myelin pathology from general pathology. In 2004, Schmierer, et al (Schmierer et al. 2004), ascribed ~90% of the magnetization transfer ratio (MTR) to myelin. While MT imaging may not necessarily be specific for myelin content, MT imaging is well known to be sensitive to changes in myelin and has become a crucial tool in clinical trials for quantitative detection of demyelination (Catalaa et al. 2000; Dousset et al. 1992; Filippi and Rocca 2004; Gass et al. 1994; Harrison, Bronskill, and Henkelman 1995; Sled and Pike 2001; Tortorella et al. 2000; Tozer et al. 2003; Yarnykh 2002; Yarnykh and Yuan 2004; Barkovich 2005; Takanashi and Barkovich 2003; Barkovich 2000), and, recently, remyelination (Chen et al. 2008). To summarize, although structures other than myelin contribute to MT, pathological changes in the MT effect of white matter are probably largely determined by changes in myelin.

Quantification of the MT effect in the Spinal Cord—The most common approach to quantify the MT effect is through the so-called magnetization transfer ratio (MTR) (Wolff and Balaban 1989), based on the ratio of image signal intensities obtained with ($S(\omega)$) and without (S_o) MT preparation at frequency ω:

$$\mathrm{MTR}(\omega)=1-\mathrm{S}(\omega)/\mathrm{S_o}$$

MTR can be thought of as the fraction of water signal saturated following an MT preparation. The MTR contrast is such that WM is bright, GM less bright, and CSF dark.

One advantage of MTR imaging is that the calculation of a ratio of two images removes contrast due to water density, T_1 and T_2 effects (water content changes, inflammation), and hardware imperfections. However, unlike diffusion parameters, it is not simple to compare MTR values between different sites or scanners, because the magnitude of the effect depends on RF power, offset, and bandwidth. In the spinal cord, calculation of an MTR faces two additional challenges. First, due to motion of the cord, the near perfect registration of the two images necessary to calculate MTR is difficult to achieve. Secondly, due to the need for high spatial resolution, the native signal to noise ratio (SNR) is low, while the calculation of a ratio between two images reduces the SNR even further (Smith et al. 2006), potentially masking contrast between tissue types, and potentially, between diseased and healthy tissue. However, if a lesion is large, and if care is taken with co-registration, it is possible to obtain MTR images of the spinal cord. An alternative method to examining MTR maps, is to obtain so-called MTR histograms (Bozzali et al. 1999; Catalaa et al. 2000; Ge et

al. 2001; Kalkers et al. 2001) at the cost of decreasing spatial information. The MTR histogram method, which examines the distribution of MTR signal intensities over the entire spinal cord segment of interest, has been shown to detect subtle differences between healthy volunteers and patients with MS (Bozzali et al. 1999), and clinically isolated syndrome (Rovaris et al. 2004); it has yet to be applied to traumatic spinal cord injury.

Another method has recently been developed for characterizing the MT effect in the spinal cord. The magnetization transfer normalized by the cerebrospinal fluid (MTCSF) approach aims to minimize the effects of cord motion, maintain the high spatial resolution necessary to explore the tracts of the spinal cord, and remove hardware dependencies, thereby facilitating inter-scanner comparison. The MTCSF approach is to quantify the MT effect from one image acquisition by normalizing an MT-weighted image by the mean signal intensity of the CSF (Smith et al. 2005). This is possible because CSF has negligible MT effect and surrounds the spinal cord. The disadvantages, however, are that since the MTCSF is calculated from only one image, T_1, T_2, and water density effects are not be eliminated, and therefore, inflammation may interfere with relating the MTCSF to myelin health. Figure 1 compares MTR, MTCSF and conventional T_1- and T_2-weighted MRI in the cervical spinal cord of a healthy volunteer (Figure 1, top row), and two patients with MS (Figure 1, middle, bottom row). Compared to the MTR and conventional T_1- and T_2-weighted MRI, the MTCSF shows excellent contrast between WM and GM; the contrast between healthy and diseased tissue can be appreciated more in the MTCSF image than in any of the other modalities. Additionally, in the patient data sets, the MTCSF most dramatically shows contrast between lesion and healthy tissue, while this distinction is difficult to appreciate on conventional T_1-, or T_2-weighted images. In contradistinction, the MTR images shows little visual signal change in these cases, reducing its appeal for studying lesions in the spinal cord.

Recent work has demonstrated that MTCSF imaging can be utilized to relate spinal cord structure to its function, as strong correlations have been reported between radiological findings with neurological deficits in patients with multiple sclerosis (Zackowski et al. 2009) and Adrenomyeloneuropathy (Fatemi et al. 2005). This approach could be applicable to other spinal cord conditions such as traumatic spinal cord injury.

Approaches for model-based quantification of the MT effect are known as quantitative MT (qMT) (Gochberg and Gore 2003; Ropele et al. 2003; Sled and Pike 2001; Stanisz et al. 2005; Yarnykh and Yuan 2004). In qMT imaging, MT-weighted images are obtained as a function of multiple MT offsets (termed the MT z-spectrum), and/or MT powers (Bryant 1996). Models wherein protons participating in the MT exchange between two (or more, (Henkelman, Stanisz, and Graham 2001; Li et al. 2008)) “pools”: a free-pool (bulk water) and one or more “not-so-free-pool(s)” (termed semi-solid, macromolecular, hydration layers, etc.) are proposed. Most often, a two-pool model is used whereby spins in a free-pool interact with the spins in a macromolecular pool. While it has been shown that the two-pool model is insufficient to explain the subtleties of the MT effect (Li et al. 2008; McLaughlin et al. 1997), for the sake of simplicity, this chapter’s examination is limited to the two-pool model. An analytical solution (Portnoy and Stanisz 2007; Sled and Pike 2001; Yarnykh 2002) to the Bloch Equations for two exchanging pools (Pike 1996) is fitted to the

experimentally determined MT z-spectra to extract one or more tissue parameters, such as: 1) the molar fraction of semi-solid protons (the bound pool fraction); 2) the rate of MT exchange (cross-relaxation rate); and 3) the transverse relaxation rate of the semi-solid protons. The advantage of estimating these parameters is that, in principle, they are physiological parameters that are independent of differences in sites, scanners, or scan parameters. These physiological parameters have been reported to reflect specific aspects of the CNS tissue: The bound pool fraction has been related to myelin density of the tissue (Henkelman, Stanisz, and Graham 2001); the rate of MT exchange has been related to the myelin composition and, in conjunction with the bound pool fraction, is reported to be able to separate dysmyelination from demyelination (Stanisz et al. 2005); the transverse relaxation rate of the bound pool is hypothesized to relate to cytotoxic cellular edema in multiple sclerosis (Stanisz et al. 2005).

While the qMT MRI approach may achieve greater specificity than MTR and MTCSF imaging, two difficulties pertain to application of qMT methods to the spinal cord: 1) prohibitively long acquisition times required to obtain the requisite sets of MT-weighted images with high spatial resolution and high signal to noise (Smith et al. 2009) and 2) the need to obtain separate absolute T_1 measurements, as well as B_1 and B_0 field maps (Ropele et al. 2003; Yarnykh 2002).

In summary, MT approaches are increasingly being applied to imaging of the spinal cord, with published reports on clinical populations, including interindividual correlations between imaging findings and neurological dysfunction. More study is needed to understand the connection between MT imaging and the pathology of interest in the spinal cord, especially in conditions where the spinal cord is the location of primary insult such as trauma.

1.2 Diffusion Tensor Imaging

In living tissues, water is not at rest, and MRI acquisitions can be sensitized to the random microscopic Brownian motion of thermally diffusing water. Diffusion-weighted (DW) MRI has been used for many years for the evaluation of ischemic brain tissue and cerebral infarcts (Sotak 2002). In structured biological tissues, the random thermal microscopic motion of water is not necessarily the same in every direction; the anisotropic properties of water diffusion can be summarized using the diffusion tensor (DT). Diffusion tensor imaging (DTI) is an extension of DW-MRI that measures the anisotropy of diffusion through application of magnetic field gradients in multiple directions (Basser and Jones 2002; Beaulieu 2002). In the brain, DTI allows for the assessment of white matter (WM) fiber bundle properties (Basser and Pierpaoli 1996; Beaulieu 2002). Recently, diffusion-weighted MRI and DTI have been applied to the cervical spinal cord (Clark and Werring 2002; Facon et al. 2005; Tsuchiya, Fujikawa, and Suzuki 2005; Wheeler-Kingshott et al. 2002), but the application of DTI to the spinal cord is still in its infancy.

DTI measures the spatial diffusion characteristics of water (Beaulieu 2002), and importantly, these diffusion characteristics are sensitive to the local composition of the biological environment, making DTI a sensitive tool to probe nervous system architecture. The metrics derived from DTI data can be quantified by scalar (orientation independent) and vector

metrics. The scalar quantities most often reported in the literature are: Fractional anisotropy (FA), which describes the degree to which the diffusion of water is directionally biased; mean diffusivity (MD) or average apparent diffusion constant (ADC_{ave}), a measure of the average water displacement; and perpendicular ($\lambda_{\perp}$) and parallel ($\lambda_{||}$) diffusivities, which describe water displacement across and along fiber pathways, respectively. Features of these contrasts that are of note include: 1) in GM, diffusion is close to isotropic, so the perpendicular and parallel diffusivities are similar to one another (low FA); 2) in WM the perpendicular diffusivity is less than the parallel diffusivity, due to myelin and axonal barriers (high FA); 3) $MD_{WM} < MD_{GM} < MD_{CSF}$. A cartoon of the contrasts and a summary of the mathematical formalism, are shown in figure 2 alongside an FA image and colormap (in which the color reports upon principle direction of diffusion, while the brightness or grayscale reports upon the magnitude of FA).

DTI has become an important imaging marker for human disease because it is sensitive to structural and tissue changes on a microscopic scale (Assaf and Cohen 1999). The diffusional displacement of water is sensitive to encounters with barriers; thus DTI metrics can reflect the nature, amount, and distribution of barriers to water. Additionally, the directional diffusivities derived from DTI data have been shown to be sensitive to and in some cases specific for axonal and myelin damage: Song et al. (Budde et al. 2008) have suggested that in an animal model of MS, parallel diffusivity may be directly related to early axonal damage prior to myelin damage, while perpendicular diffusivity can specifically report upon demyelination. However, more recent work in a model of Wallerian degeneration indicates that only reductions in parallel diffusion may be specific (Farrell JAD, Zhang J, Jones MV, DeBoy CA, Hoffman PN, Landman BA, Smith SA, Reich DS, Calabresi PA, van Zijl PCM. *Q-space and Conventional Diffusion Imaging of Axon and Myelin Damage in the Rat Spinal Cord after Axotomy*. In Press. MRM 2010). Such directional diffusivity measurements may be useful markers for following the efficacy of therapeutic interventions.

In contrast to directional diffusivities, the FA in white matter arises both from axonal and myelin (Beaulieu 2002) barriers to water diffusion. While FA is not specific for white matter damage, it has been reported to be sensitive to subtle changes in tissue health (including demyelination, dysmyelination, and axonopathy) without being confounded by inflammation. Many diseases of the central nervous system are characterized by inflammation, and the ability to assess underlying pathology without inflammation is important. Therefore, FA has been used to assess and monitor WM damage (Chenevert, Brunberg, and Pipe 1990; Horsfield and Jones 2002; Le Bihan 1995) in a number of conditions, and such studies are appearing with increasing frequency.

DTI allows characterization of mean diffusivity (MD), or the average diffusion; this is related to the DW-MRI experiments that historically preceded DTI. The MD has been valuable in characterization of the temporal evolution of stroke (Ulug et al. 1997; van Gelderen et al. 1994).

How is a DTI experiment performed, and how are DTI contrasts calculated? The diffusion tensor (DT) is a mathematical description of the diffusion process that can be estimated from

a series of diffusion-weighted MR images (Basser and Jones 2002). Typically, a diffusion-weighted (DW) image is created by applying a pair of magnetic field gradients (so-called dephasing and rephasing gradients) along one direction in 3D space. The resulting image shows signal attenuation due to the motion of water along the direction of the applied gradient; signal attenuation is proportional to the product of the water diffusivity and the diffusion time(Stejskal and Tanner 1965):

$$S(b)=s(b=0)e^{-bD}$$
$$ln\left(\frac{S(b)}{s(b=0)}\right)=-bD$$

where *b* and *D* are the applied diffusion weighting (b-value) and diffusion tensor, respectively, and *S(b=0)* is the signal in the absence of applied diffusion gradients. Note that the magnitude of $b = \gamma^2\delta^2(\Delta-\delta/3)*G$, where γ is the proton gyromagnetic ratio, δ, G, and Δ are the duration, magnitude and leading edge separation time of the diffusion weighting gradient, respectively.

The diffusion tensor is symmetric and so can be estimated from as few as 6 diffusion-weighted images, *S(b)*, acquired along non-collinear directions, plus one minimally weighted image, *S(b=0)*, often called “the b=0 image”, although the b-value, while small, is nonzero.

In addition to the scalar contrasts such as FA and MD, DTI can also yield information about the orientation of fiber pathways (Lori et al. 2002), and ultimately about the anatomical connectivity of the brain, through the use of tract-tracking, or tractography (Mori et al. 1999; Mori and van Zijl 2002). In the spinal cord, tractography may be seen as less important because the rostral-caudal orientation of fiber pathways is well known, and DTI would presumably mere confirm what we already know from neuroanatomy. However, tractography in the spinal cord provides the ability to survey each column of the spinal cord independently. Additionally, in cases such as traumatic spinal cord injury, tracts may be relocated (McDonald and Belegu 2006; McDonald and Sadowsky 2002); for instance, the rostra-caudal course may be altered upon recovery, or ongoing degeneration. An additional benefit of tractography is that for a particular fiber bundle, once tracked, it is possible to obtain fiber-related scalar metrics (Reich et al. 2006; Stieltjes et al. 2001). These metrics can be tracked along the length of the spinal cord, and related to clinical measures.

DTI is more challenging in the spinal cord than in the brain. DTI acquisitions can be prohibitively lengthy. While 6 diffusion directions are the minimum needed for estimating the DT, typically many more directions are used to increase signal to noise and reduce the variability in tensor calculations. Conventionally, as many as 30–32 gradient directions are used in performing DTI of the brain. In order to gain tract-specific information in the spinal cord, DTI acquisitions need to be of high spatial resolution, which further increases the scan time. While single-shot echo planar imaging methods are widely used to reduce scan times, these methods are highly sensitive to tissue heterogeneity, especially at boundaries between tissue types. The resulting images, therefore, can be distorted, and the resulting maps of anisotropy, etc., can be difficult to interpret.

Application of recent technical advances such as parallel imaging have allowed researchers to overcome these hindrances and study the diffusion of water in the spinal cord in disease and health (Jaermann et al. 2004). DTI data can yield scalar maps of spinal cord diffusional parameters, as well as reconstruction of spinal cord fiber pathways. Figure 3 presents DTI results in the cervical cord of a healthy volunteer, and in a patient with chronic traumatic spinal cord injury (ASIA D, C5–6 lesion epicenter). From these results, it can be seen that the four major tracts subtending the cord can be reconstructed, while slice-profiles of the scalar metrics can be compared between the site of the lesion and distal locations.

1.3 Diffusion non-Tensor Imaging (q-space)

While scalar metrics derived from DTI experiments have been the mainstay of routine DTI imaging, recent literature suggests that the directional (perpendicular, $\lambda_{\perp}$ and parallel, $\lambda_{\parallel}$) diffusivities may relate more specifically to certain types of pathology in the spinal cord (DeBoy et al. 2007; Wheeler-Kingshott and Cercignani 2009; Wheeler-Kingshott et al. 2002; Zhang et al. 2009): The diffusion of water perpendicular to axonal bundles ($\lambda_{\perp}$) is sensitive and perhaps specific for myelin loss, while the diffusion of water along the fiber bundle ($\lambda_{\parallel}$) may be specific to axonal pathology. While these metrics are easily derived from standard DTI data acquisitions, recent advances suggest that sensitivity can be improved by designing an experiment specifically to estimate these directional diffusivities. The experimental approach of applying diffusion sensitizing gradients at multiple strengths, but along few (sometimes only one) directions is known as “q-space” DWI.

As discussed in the prior section, WM axonal membranes and myelin sheaths present barriers to water, resulting in anisotropic diffusion of water (Beaulieu 2002). However, specific assignment of DWI and DTI outcome measures to axonal or myelin damage is not straightforward, in part because the biophysics of diffusion *in vivo* is not fully understood, and because axonal and myelin loss are intimately related (Farrell et al. 2008). Nevertheless, in animal models of myelin damage and axonal loss, preliminary DWI experiments sensitized to the directional diffusivity of water have drawn attention for their potential for distinguishing the different contributions of myelin and axonal membranes to the observed diffusional metrics (DeBoy et al. 2007; Zhang et al. 2009). Thus, a prevailing hypothesis is that if directional diffusivity of the injured tissue can be directly probed, then it may be possible to distinguish between myelin and axonal damage.

Multiple studies have examined this relationship in humans and in animal models. A few of the more recent studies are presented here. Q-space analysis has been used in animal models to study the effects of reduced blood flow (King et al. 1997), myelin development (Assaf, Mayk, and Cohen 2000), WM damage due to crush injury (Nossin-Manor, Duvdevani, and Cohen 2002), and myelin deficiency (Biton, Duncan, and Cohen 2006). Recently, q-space DWI has also been used to study EAE in swine spinal cords (Biton et al. 2005) and multiple sclerosis (MS) in the human brain (Assaf et al. 2002). Importantly, the microstructural information derived from q-space DWI in fixed rat spinal cords is well correlated with axon diameters obtained from histological examination (Bar-Shir and Cohen 2008). The prevailing conclusion from these studies in injured tissue is that targeted measurements of diffusivity correlate with the specific nature of the histopathology (i.e., demyelination vs.

axonal damage). In the human spinal cord, q-space approaches are of particular interest in examining the health of individual tracts, because the prevalence of lesions in many neurodegenerative diseases (such as MS) is higher than previously expected. Finally, in traumatic spinal cord injury, it may be possible to use q-space approaches to parse out the relative contributions of myelin and axonal integrity to the function of the tracts that remain.

Data Analysis Strategy/Application—The goal of "q-space" analysis is to estimate the probability density function (PDF) for water diffusion. This is the likelihood that a water molecule will be found at a certain distance from its origin, after a given time.

DW data are typically analyzed with a mono-exponential model that characterizes the observed signal decay according to the Stejskal-Tanner equation (Stejskal and Tanner 1965), consistent with the assumption that the PDF is Gaussian. Diffusion is reduced in the CNS, compared to free water, as a result of microstructural barriers. If the barriers between physiological compartments are significant, then the PDF will be non-Gaussian, and signal attenuation will become non-monoexponential, especially when using increased gradient weighting (higher b-values).

Q-space analysis (Assaf, Mayk, and Cohen 2000), unlike conventional DTI analysis, does not assume a Gaussian model for the underlying PDF. The PDF estimated from a q-space study is the conditional probability that a spin will have diffused a particular distance from its initial position during the diffusion encoding time. For a given diffusion time, a tall, narrow PDF suggests a more restricted diffusion environment, while a broader, shorter PDF suggests that diffusion is less restricted (Assaf, Mayk, and Cohen 2000; Cohen and Assaf 2002).

Analysis of *in vivo* human spinal cord q-space data has been discussed by Farrell et al. (Farrell et al. 2008). To summarize, q-space data of the human spinal cord are obtained similarly to DTI measurements. Large gradients are played out in a specific orientation with respect to the tissue of interest (i.e., perpendicular to the long axis of the spinal cord). Contrary to DTI, in which images at multiple gradient orientations are acquired at a single (non-zero) b-value, q-space imaging generally employs a single orientation but multiple b-values. To estimate the PDF, the data acquired at multiple q-values are fit to a bi-exponential signal decay curve, extrapolated, and Fourier Transformed to yield the PDF. This voxel-wise PDF then can be characterized by two parameters: the height (P0), and the width (root mean square displacement, RMSD). The height is a reflection of the probability of water not diffusing, so, if the peak is high, the interpretation is that water diffusion is restricted; water does not diffuse as far during the given diffusion time. Similarly, the RMSD can be thought of as reflecting the mobility of the water, such that a broad PDF can be interpreted as a greater freedom to diffuse. When examining q-space images (Figure 4), P0 and RMSD maps have opposing contrasts, with the former showing dark GM, and brighter WM (water is more restricted in WM), while in the latter, GM is bright and WM is dark (water diffuses less in the WM). An example of RMSD and P0 maps, and the resulting PDFs from a selection of voxels in a healthy spinal cord can be found in figure 4 (top row). Note that the PDF for white matter (blue, yellow) shows a tall, peaked, and non-Gaussian PDF (larger P0, smaller RMSD). Also, note that in GM (red), the diffusion is less restricted and thus the PDF

is lower (lower P0) and broader (larger RMSD). Therefore, the contrast is such that restricted diffusion (as occurring in WM) presents as a dark RMSD but bright P0, while less restricted diffusion (such as GM or lesion) presents as bright RMSD and darker P0. Likewise, note that CSF is brightest in RMSD images and darkest in P0.

The q-space approach is valuable because q-space metrics are sensitive to disease in both humans and animal models (Assaf, Mayk, and Cohen 2000; Song et al. 2002). An example of this is shown in Figure 4 (bottom row) where q-space derived PDFs, and RMSD and P0 maps are presented for the spinal cord of a patient with MS. In this example, the patient has a large right lateral column lesion and it can be seen that in this lesion, the PDF is shorter and wider (yellow) relative to healthy dorsal column tissue (blue). Thus, in this lesion, the P0 decreases (becoming more like GM) and the RMSD increases (water becoming less restricted).

The ability of q-space approaches to characterize the directional diffusivity of water in the CNS opens the door for this novel imaging method to be used in a variety of neurodegenerative, traumatic injured, and genetic diseases that afflict the spinal cord. Targeted imaging of the directional diffusivities may result in a more specific understanding of the pathophysiology of disease. It is possible that q-space imaging may relevant as a surrogate marker for therapeutic intervention directed at axonal protection or myelin repair.

1.4 Myelin Water Imaging

The decay rate of detectable transverse magnetization is sensitive to the local microenvironment. Conventionally, MRI data acquired from a series of spin echoes are fit to a mono-exponential decay curve. However, water contained within the myelin bilayers has an unusually rapid transverse relaxation (MacKay et al. 1994), such that the multi-echo decay of signals from all the water in a voxel would not be monoexponential. With this in mind, a technique, called multi-component T_2 relaxation MRI, has been developed, and is hypothesized to be sensitive to myelin pathology (Laule, Vavasour, Kolind et al. 2007; Laule, Vavasour, Madler et al. 2007).

Multi-echo T_2 relaxation methods have been employed to extract information about the different relaxation times (short vs. long) found when water experiences different environments within the same voxel. In WM, common models assume that two large pools of water available for imaging are water that surrounding and contained within axons (“bulk water”) and water restricted to the myelin bilayers (“myelin water”) (Laule et al. 2004; Stanisz et al. 2005). Because bulk water has a slow transverse relaxation, it is termed the “long component”, while myelin water, with a rapid transverse relaxation, is termed the “short component”. The long T_2 component is the largest, and is the major contributor to the typical tissue-specific T_2 relaxation times reported in the literature. The short component is typically much smaller, and often is invisible to conventional MRI, due to its extremely rapid transverse relaxation. However, it is this small component that is of interest due to its purported relationship to myelin content (Laule et al. 2004; Stanisz et al. 2005).

In multi-component T_2 relaxation MRI, the multi-echo signal decay curve is typically analyzed using a multi-exponential fitting routine, which generally reports upon short and

long components (Does and Snyder 1995; Webb et al. 2003). The relative amplitude of each component, and its relaxation time, are calculated.

The most common value reported from multi-exponential T_2 experiments is the "myelin water fraction" (MWF), which is the ratio of the myelin-associated water signal to the total water signal (MacKay et al. 1994; Whittall et al. 1997). The significance of the MWF, both in the brain and the spinal cord, is that it has been shown to correlate strongly with post mortem luxol fast blue staining for myelin (Whittall et al. 1997). This finding suggests that the MWF may be a surrogate marker for myelin density.

MWF imaging, and multi-component T_2 analysis, are in their infancy in the human spinal cord, where MWF imaging suffers from low signal to noise and sensitivity to motion. For instance, at low signal to noise, any curve as a function of echo time will look bi-exponential. However, recent advances in acquisition methodology have assisted in performing MWF imaging in the spinal cord, both in health and in disease (Minty et al. 2009).

As a first study, MacMillan et al. demonstrated that MWF maps could be obtained in the cervical spinal cord of healthy volunteers and patients with cervical spondylotic myelopathy (CSM), a compression-driven spinal cord degeneration that can result in remodeling of the fiber architecture of the spinal cord (ISMRM, 2008, Berlin, Germany). Images from this study are shown in figure 5 (courtesy Dr. Alex MacKay, Dr. Erin MacMillan, University of British Columbia, Vancouver, BC, Canada). In Figure 5, the T_2-weighted MRI images show a compressed spinal cord in the patient, compared to the healthy control, at the level of C3–C4. While the MWF images do not show the degree of detail that the conventional MRI does as to the location of this insult, it is interesting to note that the MWF is decreased in the patient in the left lateral column, one level caudal to the site of primary injury. As we hypothesize that MWF may be a surrogate marker for myelin health, it is possible that in this case of stenosis, the myelin is compressed and may even be remodeled. Further studies in patients with traumatic spinal cord injury and multiple sclerosis are needed to understand the temporal evolution of WM damage in each of these cases, but these preliminary results suggest the potential of using MWF as a marker for the effects of therapeutic intervention and neuroprotection.

Section 2: Functional and Metabolic Markers for Tissue Health

2.1 fMRI and Perfusion

Brain perfusion is a well-known proxy for brain health that has been imaged using Xe CT, PET, and most recently, MRI, based on the exploitation of magnetically labeled water – i.e., the magnetization of arterial water is non-invasively inverted (known as arterial spin labeling, or ASL), and the concomitant decrease in tissue water magnetization is used to measure cerebral blood flow (CBF) (Detre et al. 1992; Williams et al. 1992). Blood oxygenation level dependent (BOLD) functional MRI was introduced in the early 1990s (Menon et al. 1992; Ogawa et al. 1992; Tank, Ogawa, and Ugurbil 1992) and is now widely applied to studies of brain activation; in BOLD, deoxyhemoglobin acts as an endogenous

susceptibility contrast agent, sensitizing MRI data to reactive hyperemia (Sherrington and Roy 1890) accompanying changes in neuronal activity.

The ability to use BOLD and ASL MRI to assess spinal cord function and perfusion could improve diagnosis and help guide treatment decisions in patients with spinal cord ischemia, tumors of the spinal cord, and spinal cord injury. However, assessing spinal cord function using BOLD functional magnetic resonance imaging (fMRI) approaches has proved technically challenging (Ng et al. 2008; Stroman, Nance, and Ryner 1999).

BOLD fMRI in the brain is most commonly performed using gradient echo readouts, which provide the highest contrast-to-noise ratio (CNR) for BOLD sensitized data. However, in the spinal cord such approaches are problematic for several reasons. First, the spinal cord generates considerable local magnetic susceptibility differences due to the multiple border-zones between tissue, air, and bone. These susceptibility differences cause local magnetic field differences leading to artifacts in gradient echo acquisitions, especially at long echo time (TE). Secondly, cerebrospinal fluid pulsations cause the spinal cord to move, generating motion artifacts and spurious “activation-like” patterns. Third, typical fMRI voxels are on the order of 3 – 4 mm (isotropic) at field strengths of 1.5T and 3.0T, corresponding to only a few voxels over the width of the spinal cord (cross-sectional diameter < 15 mm) and perhaps one voxel in gray matter. Therefore, higher spatial resolution is needed. Finally, the venous architecture of the spinal cord can lead to multiple regions of false activation. Veins in the spinal cord are arranged in a network of anastomoses, consisting of a radial pattern with larger draining veins at the surface, extending both upward and downward. As the BOLD signal is not directly derived from synaptic activity, but instead from blood oxygenation changes in capillary and venous vessels, this vascular architecture can result in a distributed pattern of BOLD signal changes remote from the actually active tissue. For these reasons, alternative approaches for BOLD-based fMRI of spinal cord activation are still being developed (Stroman et al. 2003).

Imaging of spinal cord CBF using ASL MRI has also proven difficult. Spinal cord blood flow has been assessed in animal models using labeled microspheres and autoradiography (Sandler and Tator 1976; Werchan et al. 1994). Dynamic susceptibility weighted MRI techniques used for estimating perfusion in the brain (Wintermark et al. 2005) are difficult to employ in the spinal cord due to requirements for high spatial and temporal resolution. Non-invasive blood flow imaging of the spinal cord using ASL MRI approaches in rats has recently been reported (Duhamel et al. 2008); however it is hypothesized that such approaches will not transition easily to humans where cord blood flow, and therefore ASL sensitivity, are known to be significantly reduced compared to rodents. However, spinal cord blood CBF and BOLD studies hold promise in the clinical setting, as there is evidence that much of the eventual functional deficit from spinal cord injury arises from blood flow alterations that lead to ischemia and infarct, especially in the thoracic spinal cord.

2.2 Magnetic Resonance Spectroscopy

While MRI uses the nuclear magnetic resonance signals from water protons to form images, signals from other protons, such as those in metabolites, can be used to perform *in vivo* spectroscopy, or MRS. MRS has been extensively used to characterize metabolic changes

associated with neurological disease in the brain (Ross, Kreis, and Ernst 1992; Van Zijl and Barker 1997) through the quantification of concentrations of neurologically important metabolites. The three metabolites that have drawn the most attention in MRS/MRSI of the CNS are 1) N-acetyl aspartate (NAA), which has been related to axonal integrity; 2) Total choline (Cho), which changes under conditions of demyelination and gliosis; and 3) total Creatine (Cr), which is generally fairly constant (unless cerebral metabolism is altered) as it is the sum of creatine and phosphocreatine.

Application of MRS to the spinal cord has been limited (Cooke et al. 2004; Gomez-Anson et al. 2000; Kendi et al. 2004). This is due to two main factors. First, the spinal cord's small size and location (deep and surrounded by complex tissue) limits the available signal and increases the need for accurate spatial localization. The sensitivity of MRS is already orders of magnitude lower than that of conventional MRI, limiting these studies to combined assessment of WM and GM. Secondly, the magnetic susceptibility effects arising from surrounding tissues, particularly the vertebrae, makes optimization of field homogeneity within the cord, and thus separation of the resonances of the metabolites, particularly challenging.

Some MRS studies of the cervical spinal cord in humans have been performed using single voxel (SV-MRS) localization techniques. In particular, Cooke et al. (Cooke et al. 2004) have demonstrated high-resolution spectra of the cervical spinal cord in a $2.2cm^3$ voxel at 2 Tesla, yielding measures of relative concentrations of NAA, Cr, and Cho. When compared to the brain, Cooke et al. found that the relative concentrations of spinal cord metabolites are similar to those found in cerebral white matter (NAA = 14.4 mmol/l, Cr = 8.5 mmol/l, Cho = 2.3 mmol/l), with the exception of NAA, which was reported to be much higher in the spinal cord. As NAA is hypothesized to serve as a maker for neuronal density, the higher concentrations in the cord comes as no surprise, as it has been shown that spinal cord white matter has a higher density of axons than all but the most densely packed cerebral fiber pathways (e.g., corpus callosum & internal capsule).

The main limitation of SV-MRS is thus that as it does not provide information about the spatial distribution of metabolites, it cannot, in general, assess the columns that comprise the spinal cord. Alternatively, spatial information about metabolites in the columns could be obtained using MRS imaging (MRSI). Two-dimensional (2D) MRSI of water and lipids in the region of the vertebral column and spinal cord has been described, and recently Edden et al. (Edden et al. 2007) extended this approach to show that water-suppressed MRSI can be performed in the spinal cord of healthy volunteers. Similarly to the findings by Cooke, et al. (Cooke et al. 2004), the spinal cord values reported by Edden et al. are similar to those found in the brain. Interestingly, a lower NAA concentration (11.4 ± 2.8, similar to normal brain) was found in the spinal cord compared to Cooke's findings (17.3 ± 0.5).

Estimating the relative concentration of metabolites in the spinal cord may be useful not only in characterizing spinal cord pathology, but also in studying how the temporal evolution of metabolites may relate to therapeutic interventions and to neuroprotection.

Section 3: What to do when the therapeutic intervention requires placement of metal hardware for stabilization?

Surgical stabilization is the standard of care for spinal cord injury and often the methods of choice for stabilization are metallic implants such as screws and plates. While MRI, due to its excellent soft-tissue contrast, is considered to be one of the best imaging modalities to study the spinal cord, evaluate the magnitude of damage, offer prognoses, and quantify recovery, it is less effective near metal implants, due to artifacts arising from metal-induced field inhomogeneities (Ludeke, Roschmann, and Tischler 1985), gradient-induced eddy currents on metal surfaces (Graf et al. 2005), and radiofrequency shielding (Camacho, Plewes, and Henkelman 1995). In addition, local heating may induce more tissue damage.

Field inhomogeneities proximal to implanted metal result in reduced T_2* and can lead to artifacts even worse than susceptibility-driven artifacts near air-tissue interfaces. Typically spin-echo acquisitions are employed to refocus effects due to magnetic field inhomogeneities, but, due to the large gradients resulting from metal implants, even spin-echo imaging sequences may result in signal voids and spatially/slice dependent accumulation of signal (termed “signal pile-up”) (Lu et al. 2009).

Most of the advanced MRI methods presented here rely on the detection of small signal changes to characterize the microstructural integrity of the spinal cord. Obviously, metal-induced artifacts can easily interfere with such approaches. However, it has been proposed that application of “view-angle-tilting” (VAT) compensation gradients (Cho, Kim, and Kim 1988), coupled with increased RF amplitude and readout bandwidth (Butts, Pauly, and Gold 2005), can reduce artifacts near metal implants. These approaches are generally referred to as MARS (metal artifact reduction sequences) methods (Kolind et al. 2004). Addition of multiple z-phase encoding gradients for each excited slice allows for a more robust determination of the slice of interest and has been termed SEMAC (slice encoding for metal artifact correction) (Lu et al. 2009). This method can be implemented on most whole-body MRI scanners and requires little to no post-processing. The results of such an application in the cervical spine can be found in the work by Lu, Pauly, Gold, Pauly, and Hargreaves (Lu et al. 2009).

Finally, since SEMAC and other MARS strategies rely on the readout portion of the MRI sequence to be effective, it is conceivable that such readout schemes could be combined with an MT prepulse or multiple echo times (T_2 prepulse), for example, to obtain information about the MT and T_2 profiles of tissue near metallic implants. This may provide opportunities to use MRI to assess the evolution of traumatic spinal cord injury pre- and post- therapeutic intervention without being hampered by protective metal implants. However, care needs to be taken to reduce the risk of heating and related tissue damage.

Section 4: Final Comments – Sensitivity/Specificity

The goal of this chapter was to describe the important advancements in quantitative MRI of the spinal cord. However, it is important to note that many of the techniques presented have certain strengths and weaknesses, and furthermore, are sensitive to various aspects of tissue

pathology. To that end, Table 1 summarizes the sensitivity of each technique (where a + indicates sensitivity) to 1) myelin changes, 2) axonal changes, and 3) inflammation. Caution should be taken in interpretation of this table as many pathologies of the human nervous system are a combination of axonal, myelin, and inflammatory changes, and to date, no quantitative MRI technique has been reported to be perfectly specific for the pathologies listed. One final point of caution to the reader is that even though the relative sensitivity of each of these techniques is presented, there is significant debate in the literature as to which techniques are more (or less) sensitive than the others.

Section 5: Conclusion

Advanced MRI approaches shed important light on the brain, but have not been widely applied to the spinal cord, primarily because of the cord's small cross-sectional size, location within structures of varying magnetic susceptibility, and motion induced by CSF pulsations. However, recently progress has been made in applying advanced approaches (such as MT & DTI) to the spinal cord. As the gross anatomy of the cord, particularly the distribution of fiber pathways, is well known, advanced MRI of the spinal cord may offer the ability to relate structure and function with great specificity. Future advances will no doubt provide a wealth of information about disease in the cord, and potentially, offer support for prognostic evaluation and therapeutic monitoring in cord diseases and damage.

Glossary of Terms/Abbreviations

2D	Two Dimensional
ADC	Apparent Diffusion Constant
ASL	Arterial Spin Labeling
BOLD	Blood Oxygenation Level Dependent
CBF	Cerebral Blood Flow
Cho	Choline
CNR	Contrast to Noise Ratio
CNS	Central Nervous System
Cr	Creatine
CSF	Cerebrospinal Fluid
CT	Computed Tomography
D	Diffusion Gradient Spacing
d	Duration of Diffusion Gradient
DT	Diffusion Tensor
DTI	Diffusion Tensor Imaging
DW	Diffusion Weighted

EAE	Experimental Autoimmune Encephalomyelitis
EPI	Echo Planar Imaging
FA	Fractional Anisotropy
FLAIR	Fluid Attenuated Inversion Recovery
fMRI	Functional MRI
g	Gyromagnetic Ratio
GM	Gray Matter
HARDI	High Angular Resolution Diffusion Imaging
$\lambda_{\perp}$	Perpendicular Diffusivity
$\lambda_{\parallel}$	Parallel Diffusivity
MARS	Metal Artifact Reduction Sequences
MD	Mean Diffusivity
MRI	Magnetic Resonance Imaging
MRS	Magnetic Resonance Spectroscopy
MRSI	Magnetic Resonance Spectroscopic Imaging
MS	Multiple Sclerosis
MT	Magnetization Transfer
MTCSF	MT Normalized to CSF
MTR	Magnetization Transfer Ratio
MWF	Myelin Water Fraction
NAA	N-Acetyl Aspartate
P0	Height of the PDF
PDF	Probability Density Function
PET	Positron Emission Tomography
qMT	Quantitative MT
RF	Radio Frequency
RMSD	Room Mean Square Displacement
SEMAC	Slice Encoding for Metal Artifact Correction
SNR	Signal to Noise Ratio
SSFP	Steady State Free Precession
SV-MRS	Single Voxel MRS
T	Tesla

T1	Longitudinal Relaxation
T2	Transverse Relaxation
TE	Echo Time
VAT	View-angle-tilting
Voxel	Volume Element
WM	White Matter

References Cited

Assaf Y, Ben-Bashat D, Chapman J, Peled S, Biton IE, Kafri M, Segev Y, Hendler T, Korczyn AD, Graif M, Cohen Y. High b-value q-space analyzed diffusion-weighted MRI: application to multiple sclerosis. Magn Reson Med. 2002; 47(1):115–26. [PubMed: 11754450]

Assaf Y, Cohen Y. Structural information in neuronal tissue as revealed by q-space diffusion NMR spectroscopy of metabolites in bovine optic nerve. NMR Biomed. 1999; 12(6):335–44. [PubMed: 10516615]

Assaf Y, Mayk A, Cohen Y. Displacement imaging of spinal cord using q-space diffusion-weighted MRI. Magn Reson Med. 2000; 44(5):713–22. [PubMed: 11064406]

Bar-Shir A, Cohen Y. High b-value q-space diffusion MRS of nerves: structural information and comparison with histological evidence. NMR Biomed. 2008; 21(2):165–74. [PubMed: 17492659]

Barkovich AJ. Concepts of myelin and myelination in neuroradiology. AJNR Am J Neuroradiol. 2000; 21(6):1099–109. [PubMed: 10871022]

Barkovich AJ. Magnetic resonance techniques in the assessment of myelin and myelination. J Inherit Metab Dis. 2005; 28(3):311–43. [PubMed: 15868466]

Basser PJ, Jones DK. Diffusion-tensor MRI: theory, experimental design and data analysis – a technical review. NMR Biomed. 2002; 15(7–8):456–67. [PubMed: 12489095]

Basser PJ, Mattiello J, LeBihan D. MR diffusion tensor spectroscopy and imaging. Biophys J. 1994; 66(1):259–67. [PubMed: 8130344]

Basser PJ, Pierpaoli C. Microstructural and physiological features of tissues elucidated by quantitative-diffusion-tensor MRI. J Magn Reson B. 1996; 111(3):209–19. [PubMed: 8661285]

Bastos Leite AJ, Scheltens P, Barkhof F. Pathological aging of the brain: an overview. Top Magn Reson Imaging. 2004; 15(6):369–89. [PubMed: 16041289]

Beaulieu C. The basis of anisotropic water diffusion in the nervous system – a technical review. NMR Biomed. 2002; 15(7–8):435–55. [PubMed: 12489094]

Biton IE I, Duncan D, Cohen Y. High b-value q-space diffusion MRI in myelin-deficient rat spinal cords. Magn Reson Imaging. 2006; 24(2):161–6. [PubMed: 16455404]

Biton IE, Mayk A, Kidron D, Assaf Y, Cohen Y. Improved detectability of experimental allergic encephalomyelitis in excised swine spinal cords by high b-value q-space DWI. Exp Neurol. 2005; 195(2):437–46. [PubMed: 16098966]

Bozzali M, Rocca MA, Iannucci G, Pereira C, Comi G, Filippi M. Magnetization-transfer histogram analysis of the cervical cord in patients with multiple sclerosis. AJNR Am J Neuroradiol. 1999; 20(10):1803–8. [PubMed: 10588100]

Bryant RG. The dynamics of water-protein interactions. Annu Rev Biophys Biomol Struct. 1996; 25:29–53. [PubMed: 8800463]

Budde MD, Kim JH, Liang HF, Russell JH, Cross AH, Song SK. Axonal injury detected by in vivo diffusion tensor imaging correlates with neurological disability in a mouse model of multiple sclerosis. NMR Biomed. 2008; 21(6):589–97. [PubMed: 18041806]

Butts K, Pauly JM, Gold GE. Reduction of blurring in view angle tilting MRI. Magn Reson Med. 2005; 53(2):418–24. [PubMed: 15678535]

Bydder GM, Steiner RE. NMR imaging of the brain. Neuroradiology. 1982; 23(5):231–40. [PubMed: 7121818]

Camacho CR, Plewes DB, Henkelman RM. Nonsusceptibility artifacts due to metallic objects in MR imaging. J Magn Reson Imaging. 1995; 5(1):75–88. [PubMed: 7696813]

Catalaa I, Grossman RI, Kolson DL, Udupa JK, Nyul LG, Wei L, Zhang X, Polansky M, Mannon LJ, McGowan JC. Multiple sclerosis: magnetization transfer histogram analysis of segmented normal-appearing white matter. Radiology. 2000; 216(2):351–5. [PubMed: 10924552]

Chen JT, Collins DL, Atkins HL, Freedman MS, Arnold DL. Magnetization transfer ratio evolution with demyelination and remyelination in multiple sclerosis lesions. Ann Neurol. 2008; 63(2):254–62. [PubMed: 18257039]

Chenevert TL, Brunberg JA, Pipe JG. Anisotropic diffusion in human white matter: demonstration with MR techniques in vivo. Radiology. 1990; 177(2):401–5. [PubMed: 2217776]

Cho ZH, Kim DJ, Kim YK. Total inhomogeneity correction including chemical shifts and susceptibility by view angle tilting. Med Phys. 1988; 15(1):7–11. [PubMed: 3352554]

Clark CA, Werring DJ. Diffusion tensor imaging in spinal cord: methods and applications – a review. NMR Biomed. 2002; 15(7–8):578–86. [PubMed: 12489104]

Cohen Y, Assaf Y. High b-value q-space analyzed diffusion-weighted MRS and MRI in neuronal tissues – a technical review. NMR Biomed. 2002; 15(7–8):516–42. [PubMed: 12489099]

Cohen-Adad J, Descoteaux M, Rossignol S, Hoge RD, Deriche R, Benali H. Detection of multiple pathways in the spinal cord using q-ball imaging. Neuroimage. 2008; 42(2):739–49. [PubMed: 18562214]

Cooke FJ, Blamire AM, Manners DN, Styles P, Rajagopalan B. Quantitative proton magnetic resonance spectroscopy of the cervical spinal cord. Magn Reson Med. 2004; 51(6):1122–8. [PubMed: 15170831]

De Coene B, Hajnal JV, Gatehouse P, Longmore DB, White SJ, Oatridge A, Pennock JM, Young IR, Bydder GM. MR of the brain using fluid-attenuated inversion recovery (FLAIR) pulse sequences. AJNR Am J Neuroradiol. 1992; 13(6):1555–64. [PubMed: 1332459]

DeBoy CA, Zhang J, Dike S, Shats I, Jones M, Reich DS, Mori S, Nguyen T, Rothstein B, Miller RH, Griffin JT, Kerr DA, Calabresi PA. High resolution diffusion tensor imaging of axonal damage in focal inflammatory and demyelinating lesions in rat spinal cord. Brain. 2007; 130(Pt 8):2199–210. [PubMed: 17557778]

Deibler AR, Pollock JM, Kraft RA, Tan H, Burdette JH, Maldjian JA. Arterial spin-labeling in routine clinical practice, part 1: technique and artifacts. AJNR Am J Neuroradiol. 2008; 29(7):1228–34. [PubMed: 18372417]

Deibler AR, Pollock JM, Kraft RA, Tan H, Burdette JH, Maldjian JA. Arterial spin-labeling in routine clinical practice, part 2: hypoperfusion patterns. AJNR Am J Neuroradiol. 2008; 29(7):1235–41. [PubMed: 18356467]

Deibler AR, Pollock JM, Kraft RA, Tan H, Burdette JH, Maldjian JA. Arterial spin-labeling in routine clinical practice, part 3: hyperperfusion patterns. AJNR Am J Neuroradiol. 2008; 29(8):1428–35. [PubMed: 18356466]

Detre JA, Leigh JS, Williams DS, Koretsky AP. Perfusion imaging. Magn Reson Med. 1992; 23(1): 37–45. [PubMed: 1734182]

Does MD, Snyder RE. T2 relaxation of peripheral nerve measured in vivo. Magn Reson Imaging. 1995; 13(4):575–80. [PubMed: 7674853]

Dousset V, Grossman RI, Ramer KN, Schnall MD, Young LH, Gonzalez-Scarano F, Lavi E, Cohen JA. Experimental allergic encephalomyelitis and multiple sclerosis: lesion characterization with magnetization transfer imaging. Radiology. 1992; 182(2):483–91. [PubMed: 1732968]

Duhamel G, Callot V, Cozzone PJ, Kober F. Spinal cord blood flow measurement by arterial spin labeling. Magn Reson Med. 2008; 59(4):846–54. [PubMed: 18383283]

Edden RA, Bonekamp D, Smith MA, Dubey P, Barker PB. Proton MR spectroscopic imaging of the medulla and cervical spinal cord. J Magn Reson Imaging. 2007; 26(4):1101–5. [PubMed: 17896355]

Facon D, Ozanne A, Fillard P, Lepeintre JF, Tournoux-Facon C, Ducreux D. MR diffusion tensor imaging and fiber tracking in spinal cord compression. AJNR Am J Neuroradiol. 2005; 26(6): 1587–94. [PubMed: 15956535]

Farrell JA, Smith SA, Gordon-Lipkin EM, Reich DS, Calabresi PA, van Zijl PC. High b-value q-space diffusion-weighted MRI of the human cervical spinal cord in vivo: feasibility and application to multiple sclerosis. Magn Reson Med. 2008; 59(5):1079–89. [PubMed: 18429023]

Fatemi A, Smith SA, Dubey P, Zackowski KM, Bastian AJ, van Zijl PC, Moser HW, Raymond GV, Golay X. Magnetization transfer MRI demonstrates spinal cord abnormalities in adrenomyeloneuropathy. Neurology. 2005; 64(10):1739–45. [PubMed: 15911801]

Filippi M, Rocca MA. Magnetization transfer magnetic resonance imaging in the assessment of neurological diseases. J Neuroimaging. 2004; 14(4):303–13. [PubMed: 15358949]

Gass A, Barker GJ, Kidd D, Thorpe JW, MacManus D, Brennan A, Tofts PS, Thompson AJ, McDonald WI, Miller DH. Correlation of magnetization transfer ratio with clinical disability in multiple sclerosis. Ann Neurol. 1994; 36(1):62–7. [PubMed: 8024264]

Ge Y, Grossman RI, Udupa JK, Babb JS, Kolson DL, McGowan JC. Magnetization transfer ratio histogram analysis of gray matter in relapsing-remitting multiple sclerosis. AJNR Am J Neuroradiol. 2001; 22(3):470–5. [PubMed: 11237968]

Gochberg DF, Gore JC. Quantitative imaging of magnetization transfer using an inversion recovery sequence. Magn Reson Med. 2003; 49(3):501–5. [PubMed: 12594753]

Gomez-Anson B, MacManus DG, Parker GJ, Davie CA, Barker GJ, Moseley IF, McDonald WI, Miller DH. In vivo 1H-magnetic resonance spectroscopy of the spinal cord in humans. Neuroradiology. 2000; 42(7):515–7. [PubMed: 10952184]

Graf H, Steidle G, Martirosian P, Lauer UA, Schick F. Metal artifacts caused by gradient switching. Magn Reson Med. 2005; 54(1):231–4. [PubMed: 15968663]

Grossman RI, Gonzalez-Scarano F, Atlas SW, Galetta S, Silberberg DH. Multiple sclerosis: gadolinium enhancement in MR imaging. Radiology. 1986; 161(3):721–5. [PubMed: 3786722]

Hagmann P, Jonasson L, Maeder P, Thiran JP, Wedeen VJ, Meuli R. Understanding diffusion MR imaging techniques: from scalar diffusion-weighted imaging to diffusion tensor imaging and beyond. Radiographics. 2006; 26(Suppl 1):S205–23. [PubMed: 17050517]

Hajnal JV, Bryant DJ, Kasuboski L, Pattany PM, De Coene B, Lewis PD, Pennock JM, Oatridge A, Young IR, Bydder GM. Use of fluid attenuated inversion recovery (FLAIR) pulse sequences in MRI of the brain. J Comput Assist Tomogr. 1992; 16(6):841–4. [PubMed: 1430427]

Harrison R, Bronskill MJ, Henkelman RM. Magnetization transfer and T2 relaxation components in tissue. Magn Reson Med. 1995; 33(4):490–6. [PubMed: 7776879]

Henkelman RM, Stanisz GJ, Graham SJ. Magnetization transfer in MRI: a review. NMR Biomed. 2001; 14(2):57–64. [PubMed: 11320533]

Horsfield MA, Jones DK. Applications of diffusion-weighted and diffusion tensor MRI to white matter diseases – a review. NMR Biomed. 2002; 15(7–8):570–7. [PubMed: 12489103]

Huk W, Heindel W. Nuclear magnetic resonance (NMR) imaging in diseases of the central nervous system: initial results. Radiat Med. 1983; 1(2):105–11. [PubMed: 6679902]

Jaermann T, Crelier G, Pruessmann KP, Golay X, Netsch T, van Muiswinkel AM, Mori S, van Zijl PC, Valavanis A, Kollias S, Boesiger P. SENSE-DTI at 3 T. Magn Reson Med. 2004; 51(2):230–6. [PubMed: 14755645]

Kalkers NF, Hintzen RQ, van Waesberghe JH, Lazeron RH, van Schijndel RA, Ader HJ, Polman CH, Barkhof F. Magnetization transfer histogram parameters reflect all dimensions of MS pathology, including atrophy. J Neurol Sci. 2001; 184(2):155–62. [PubMed: 11239950]

Kendi AT, Tan FU, Kendi M, Yilmaz S, Huvaj S, Tellioglu S. MR spectroscopy of cervical spinal cord in patients with multiple sclerosis. Neuroradiology. 2004; 46(9):764–9. [PubMed: 15258708]

King MD, Houseman J, Gadian DG, Connelly A. Localized q-space imaging of the mouse brain. Magn Reson Med. 1997; 38(6):930–7. [PubMed: 9402194]

Kolind SH, MacKay AL, Munk PL, Xiang QS. Quantitative evaluation of metal artifact reduction techniques. J Magn Reson Imaging. 2004; 20(3):487–95. [PubMed: 15332257]

Laule C I, Vavasour M, Kolind SH, Traboulsee AL, Moore GR, Li DK, Mackay AL. Long T2 water in multiple sclerosis: what else can we learn from multi-echo T2 relaxation? J Neurol. 2007; 254(11): 1579–87. [PubMed: 17762945]

Laule C, Vavasour IM, Madler B, Kolind SH, Sirrs SM, Brief EE, Traboulsee AL, Moore GR, Li DK, MacKay AL. MR evidence of long T2 water in pathological white matter. J Magn Reson Imaging. 2007; 26(4):1117–21. [PubMed: 17896375]

Laule C I, Vavasour M, Moore GR, Oger J, Li DK, Paty DW, MacKay AL. Water content and myelin water fraction in multiple sclerosis. A T2 relaxation study. J Neurol. 2004; 251(3):284–93. [PubMed: 15015007]

Le Bihan D. Molecular diffusion, tissue microdynamics and microstructure. NMR Biomed. 1995; 8(7–8):375–86. [PubMed: 8739274]

Li AX, Hudson RH, Barrett JW, Jones CK, Pasternak SH, Bartha R. Four-pool modeling of proton exchange processes in biological systems in the presence of MRI-paramagnetic chemical exchange saturation transfer (PARACEST) agents. Magn Reson Med. 2008; 60(5):1197–206. [PubMed: 18958857]

Lori NF, Akbudak E, Shimony JS, Cull TS, Snyder AZ, Guillory RK, Conturo TE. Diffusion tensor fiber tracking of human brain connectivity: aquisition methods, reliability analysis and biological results. NMR Biomed. 2002; 15(7–8):494–515. [PubMed: 12489098]

Lu W, Pauly KB, Gold GE, Pauly JM, Hargreaves BA. SEMAC: Slice Encoding for Metal Artifact Correction in MRI. Magn Reson Med. 2009; 62(1):66–76. [PubMed: 19267347]

Ludeke KM, Roschmann P, Tischler R. Susceptibility artefacts in NMR imaging. Magn Reson Imaging. 1985; 3(4):329–43. [PubMed: 4088009]

MacKay A, Whittall K, Adler J, Li D, Paty D, Graeb D. In vivo visualization of myelin water in brain by magnetic resonance. Magn Reson Med. 1994; 31(6):673–7. [PubMed: 8057820]

Mansfield P. Real-time echo-planar imaging by NMR. Br Med Bull. 1984; 40(2):187–90. [PubMed: 6744006]

McDonald JW, Belegu V. Demyelination and remyelination after spinal cord injury. J Neurotrauma. 2006; 23(3–4):345–59. [PubMed: 16629621]

McDonald JW, Sadowsky C. Spinal-cord injury. Lancet. 2002; 359(9304):417–25. [PubMed: 11844532]

McLaughlin AC, Ye FQ, Pekar JJ, Santha AK, Frank JA. Effect of magnetization transfer on the measurement of cerebral blood flow using steady-state arterial spin tagging approaches: a theoretical investigation. Magn Reson Med. 1997; 37(4):501–10. [PubMed: 9094071]

Melhem ER, Mori S, Mukundan G, Kraut MA, Pomper MG, van Zijl PC. Diffusion tensor MR imaging of the brain and white matter tractography. AJR Am J Roentgenol. 2002; 178(1):3–16. [PubMed: 11756078]

Menon RS, Ogawa S, Kim SG, Ellermann JM, Merkle H, Tank DW, Ugurbil K. Functional brain mapping using magnetic resonance imaging. Signal changes accompanying visual stimulation. Invest Radiol. 1992; 27(Suppl 2):S47–53. [PubMed: 1468875]

Minty EP, Bjarnason TA, Laule C, MacKay AL. Myelin water measurement in the spinal cord. Magn Reson Med. 2009; 61(4):883–92. [PubMed: 19191283]

Mori S, Crain BJ, Chacko VP, van Zijl PC. Three-dimensional tracking of axonal projections in the brain by magnetic resonance imaging. Ann Neurol. 1999; 45(2):265–9. [PubMed: 9989633]

Mori S, van Zijl PC. Fiber tracking: principles and strategies – a technical review. NMR Biomed. 2002; 15(7–8):468–80. [PubMed: 12489096]

Morrison C, Henkelman RM. A model for magnetization transfer in tissues. Magn Reson Med. 1995; 33(4):475–82. [PubMed: 7776877]

Moseley ME, Wendland MF, Kucharczyk J. Magnetic resonance imaging of diffusion and perfusion. Top Magn Reson Imaging. 1991; 3(3):50–67. [PubMed: 2054198]

Ng MC, Wu EX, Lau HF, Hu Y, Lam EY, Luk KD. Cervical spinal cord BOLD fMRI study: modulation of functional activation by dexterity of dominant and non-dominant hands. Neuroimage. 2008; 39(2):825–31. [PubMed: 17962042]

Nossin-Manor R, Duvdevani R, Cohen Y. q-Space high b value diffusion MRI of hemi-crush in rat spinal cord: evidence for spontaneous regeneration. Magn Reson Imaging. 2002; 20(3):231–41. [PubMed: 12117605]

Ogawa S, Tank DW, Menon R, Ellermann JM, Kim SG, Merkle H, Ugurbil K. Intrinsic signal changes accompanying sensory stimulation: functional brain mapping with magnetic resonance imaging. Proc Natl Acad Sci U S A. 1992; 89(13):5951–5. [PubMed: 1631079]

Pike GB. Pulsed magnetization transfer contrast in gradient echo imaging: a two-pool analytic description of signal response. Magn Reson Med. 1996; 36(1):95–103. [PubMed: 8795027]

Portnoy S, Stanisz GJ. Modeling pulsed magnetization transfer. Magn Reson Med. 2007; 58(1):144–55. [PubMed: 17659607]

Reich DS, Smith SA, Jones CK, Zackowski KM, van Zijl PC, Calabresi PA, Mori S. Quantitative characterization of the corticospinal tract at 3T. AJNR Am J Neuroradiol. 2006; 27(10):2168–78. [PubMed: 17110689]

Rodrigo S, Henry-Feugeas MC, Oppenheim C, Verny M, Meder JF, Fredy D. Imaging of dementia with magnetic resonance. Presse Med. 2004; 33(15):1027–33. [PubMed: 15523253]

Ropele S, Seifert T, Enzinger C, Fazekas F. Method for quantitative imaging of the macromolecular 1H fraction in tissues. Magn Reson Med. 2003; 49(5):864–71. [PubMed: 12704769]

Ross B, Kreis R, Ernst T. Clinical tools for the 90s: magnetic resonance spectroscopy and metabolite imaging. Eur J Radiol. 1992; 14(2):128–40. [PubMed: 1563413]

Rovaris M, Gallo A, Riva R, Ghezzi A, Bozzali M, Benedetti B, Martinelli V, Falini A, Comi G, Filippi M. An MT MRI study of the cervical cord in clinically isolated syndromes suggestive of MS. Neurology. 2004; 63(3):584–5. [PubMed: 15304603]

Sandler AN, Tator CH. Review of the measurement of normal spinal cord blood flow. Brain Res. 1976; 118(2):181–98. [PubMed: 826305]

Schmierer K, Scaravilli F, Altmann DR, Barker GJ, Miller DH. Magnetization transfer ratio and myelin in postmortem multiple sclerosis brain. Ann Neurol. 2004; 56(3):407–15. [PubMed: 15349868]

Scotti G, Scialfa G, Biondi A, Landoni L, Caputo D, Cazzullo CL. Magnetic resonance in multiple sclerosis. Neuroradiology. 1986; 28(4):319–23. [PubMed: 3762909]

Sevick RJ, Kucharczyk J, Mintorovitch J, Moseley ME, Derugin N, Norman D. Diffusion-weighted MR imaging and T2-weighted MR imaging in acute cerebral ischaemia: comparison and correlation with histopathology. Acta Neurochir Suppl (Wien). 1990; 51:210–2. [PubMed: 1708645]

Sherrington CS, Roy CS. On the Regulation of Blood-supply of the Brain. J Physiol. 1890; 11(1–2): 85–158.

Sled JG, Pike GB. Quantitative imaging of magnetization transfer exchange and relaxation properties in vivo using MRI. Magn Reson Med. 2001; 46(5):923–31. [PubMed: 11675644]

Smith SA, Farrell JA, Jones CK, Reich DS, Calabresi PA, van Zijl PC. Pulsed magnetization transfer imaging with body coil transmission at 3 Tesla: feasibility and application. Magn Reson Med. 2006; 56(4):866–75. [PubMed: 16964602]

Smith SA, Golay X, Fatemi A, Jones CK, Raymond GV, Moser HW, van Zijl PC. Magnetization transfer weighted imaging in the upper cervical spinal cord using cerebrospinal fluid as intersubject normalization reference (MTCSF imaging). Magn Reson Med. 2005; 54(1):201–6. [PubMed: 15968676]

Smith SA, Golay X, Fatemi A, Mahmood A, Raymond GV, Moser HW, van Zijl PC, Stanisz GJ. Quantitative magnetization transfer characteristics of the human cervical spinal cord in vivo: application to adrenomyeloneuropathy. Magn Reson Med. 2009; 61(1):22–7. [PubMed: 19097204]

Song SK, Sun SW, Ramsbottom MJ, Chang C, Russell J, Cross AH. Dysmyelination revealed through MRI as increased radial (but unchanged axial) diffusion of water. Neuroimage. 2002; 17(3):1429–36. [PubMed: 12414282]

Sotak CH. The role of diffusion tensor imaging in the evaluation of ischemic brain injury – a review. NMR Biomed. 2002; 15(7–8):561–9. [PubMed: 12489102]

Stanisz GJ, Kecojevic A, Bronskill MJ, Henkelman RM. Characterizing white matter with magnetization transfer and T(2). Magn Reson Med. 1999; 42(6):1128–36. [PubMed: 10571935]

Stanisz GJ, Odrobina EE, Pun J, Escaravage M, Graham SJ, Bronskill MJ, Henkelman RM. T1, T2 relaxation and magnetization transfer in tissue at 3T. Magn Reson Med. 2005; 54(3):507–12. [PubMed: 16086319]

Stejskal EO, Tanner JE. Spin diffusion measurements: spin echoes in the presence of a time-dependent field gradient. J Phys Chem. 1965; 42:288–292.

Stieltjes B, Kaufmann WE, van Zijl PC, Fredericksen K, Pearlson GD, Solaiyappan M, Mori S. Diffusion tensor imaging and axonal tracking in the human brainstem. Neuroimage. 2001; 14(3): 723–35. [PubMed: 11506544]

Stroman PW, Nance PW, Ryner LN. BOLD MRI of the human cervical spinal cord at 3 tesla. Magn Reson Med. 1999; 42(3):571–6. [PubMed: 10467302]

Stroman PW, Tomanek B, Krause V, Frankenstein UN, Malisza KL. Functional magnetic resonance imaging of the human brain based on signal enhancement by extravascular protons (SEEP fMRI). Magn Reson Med. 2003; 49(3):433–9. [PubMed: 12594745]

Takanashi J, Barkovich AJ. The changing MR imaging appearance of polymicrogyria: a consequence of myelination. AJNR Am J Neuroradiol. 2003; 24(5):788–93. [PubMed: 12748072]

Tank DW, Ogawa S, Ugurbil K. Mapping the brain with MRI. Curr Biol. 1992; 2(10):525–8. [PubMed: 15336045]

Tortorella C, Viti B, Bozzali M, Sormani MP, Rizzo G, Gilardi MF, Comi G, Filippi M. A magnetization transfer histogram study of normal-appearing brain tissue in MS. Neurology. 2000; 54(1):186–93. [PubMed: 10636146]

Tozer D, Ramani A, Barker GJ, Davies GR, Miller DH, Tofts PS. Quantitative magnetization transfer mapping of bound protons in multiple sclerosis. Magn Reson Med. 2003; 50(1):83–91. [PubMed: 12815682]

Tsuchiya K, Fujikawa A, Suzuki Y. Diffusion tractography of the cervical spinal cord by using parallel imaging. AJNR Am J Neuroradiol. 2005; 26(2):398–400. [PubMed: 15709143]

Tuch DS. Q-ball imaging. Magn Reson Med. 2004; 52(6):1358–72. [PubMed: 15562495]

Ulug AM, Beauchamp N Jr, Bryan RN, van Zijl PC. Absolute quantitation of diffusion constants in human stroke. Stroke. 1997; 28(3):483–90. [PubMed: 9056600]

van Gelderen P, de Vleeschouwer MH, DesPres D, Pekar J, van Zijl PC, Moonen CT. Water diffusion and acute stroke. Magn Reson Med. 1994; 31(2):154–63. [PubMed: 8133751]

Van Zijl PC, Barker PB. Magnetic resonance spectroscopy and spectroscopic imaging for the study of brain metabolism. Ann N Y Acad Sci. 1997; 820:75–96. [PubMed: 9237450]

Webb S, Munro CA, Midha R, Stanisz GJ. Is multicomponent T2 a good measure of myelin content in peripheral nerve? Magn Reson Med. 2003; 49(4):638–45. [PubMed: 12652534]

Werchan PM, Schadt JC, Fanton JW, Laughlin MH. Cerebral and spinal cord blood flow dynamics during high sustained +Gz. Aviat Space Environ Med. 1994; 65(6):501–9. [PubMed: 8074622]

Wheeler-Kingshott CA, Cercignani M. About “axial” and “radial” diffusivities. Magn Reson Med. 2009

Wheeler-Kingshott CA, Hickman SJ, Parker GJ, Ciccarelli O, Symms MR, Miller DH, Barker GJ. Investigating cervical spinal cord structure using axial diffusion tensor imaging. Neuroimage. 2002; 16(1):93–102. [PubMed: 11969321]

White SJ, Hajnal JV, Young IR, Bydder GM. Use of fluid-attenuated inversion-recovery pulse sequences for imaging the spinal cord. Magn Reson Med. 1992; 28(1):153–62. [PubMed: 1435218]

Whittall KP, MacKay AL, Graeb DA, Nugent RA, Li DK, Paty DW. In vivo measurement of T2 distributions and water contents in normal human brain. Magn Reson Med. 1997; 37(1):34–43. [PubMed: 8978630]

Williams DS, Detre JA, Leigh JS, Koretsky AP. Magnetic resonance imaging of perfusion using spin inversion of arterial water. Proc Natl Acad Sci U S A. 1992; 89(1):212–6. [PubMed: 1729691]

Wintermark M, Sesay M, Barbier E, Borbely K, Dillon WP, Eastwood JD, Glenn TC, Grandin CB, Pedraza S, Soustiel JF, Nariai T, Zaharchuk G, Caille JM, Dousset V, Yonas H. Comparative overview of brain perfusion imaging techniques. Stroke. 2005; 36(9):e83–99. [PubMed: 16100027]

Wolff SD, Balaban RS. Magnetization transfer contrast (MTC) and tissue water proton relaxation in vivo. Magn Reson Med. 1989; 10(1):135–44. [PubMed: 2547135]

Wu YC, Alexander AL. Hybrid diffusion imaging. Neuroimage. 2007; 36(3):617–29. [PubMed: 17481920]

Yarnykh VL. Pulsed Z-spectroscopic imaging of cross-relaxation parameters in tissues for human MRI: theory and clinical applications. Magn Reson Med. 2002; 47(5):929–39. [PubMed: 11979572]

Yarnykh VL, Yuan C. Cross-relaxation imaging reveals detailed anatomy of white matter fiber tracts in the human brain. Neuroimage. 2004; 23(1):409–24. [PubMed: 15325389]

Zackowski KM, Smith SA, Reich DS, Gordon-Lipkin E, Chodkowski BA, Sambandan DR, Shteyman M, Bastian AJ, van Zijl PC, Calabresi PA. Sensorimotor dysfunction in multiple sclerosis and column-specific magnetization transfer-imaging abnormalities in the spinal cord. Brain. 2009; 132(Pt 5):1200–9. [PubMed: 19297508]

Zhang J, Jones M, DeBoy CA, Reich DS, Farrell JA, Hoffman PN, Griffin JW, Sheikh KA, Miller MI, Mori S, Calabresi PA. Diffusion tensor magnetic resonance imaging of Wallerian degeneration in rat spinal cord after dorsal root axotomy. J Neurosci. 2009; 29(10):3160–71. [PubMed: 19279253]

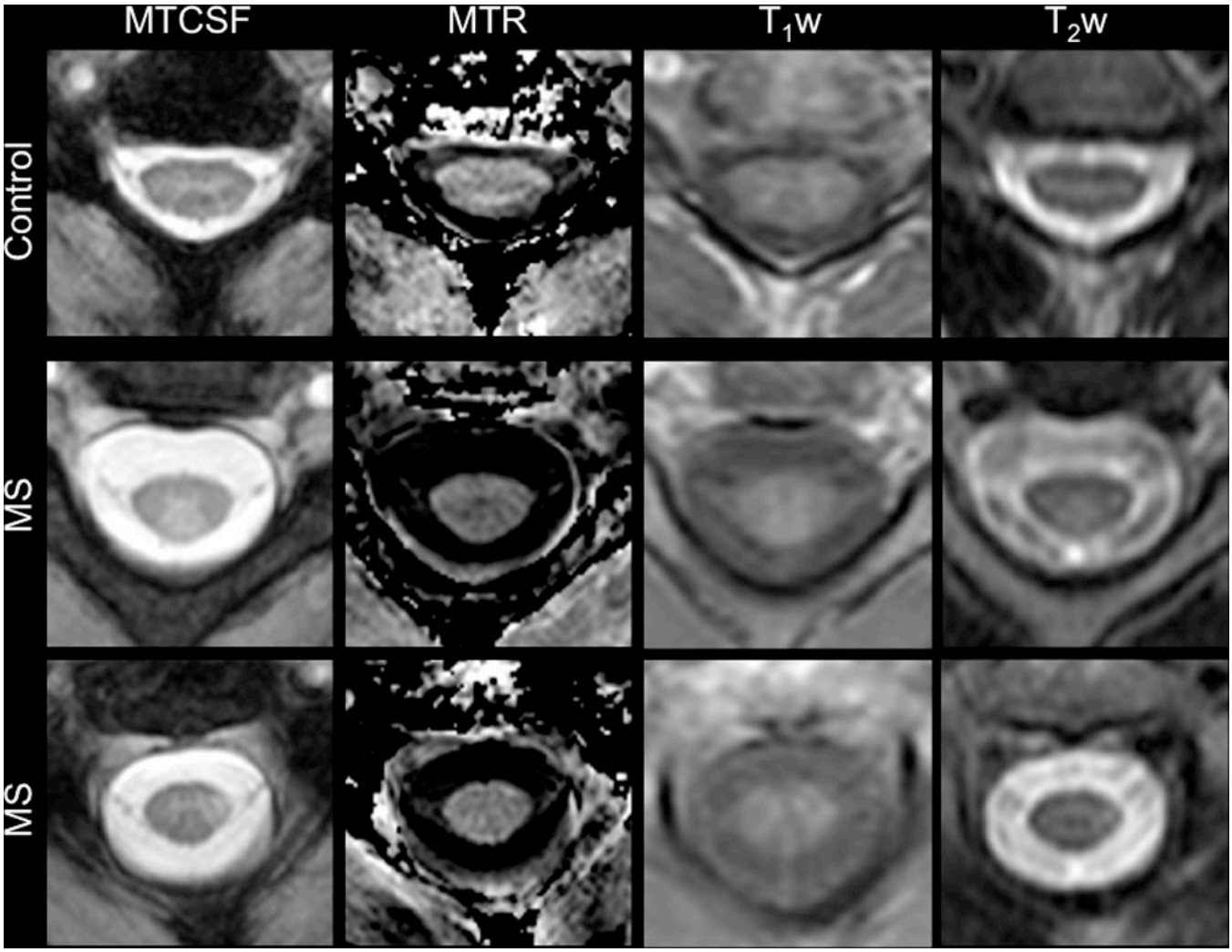

Figure 1.

Comparison of MTCSF, MTR, T_1-weighted, and T_2-weighted imaging in the cervical spinal cord of a healthy control (top) and two patients with multiple sclerosis (bottom two panels). In the MTCSF images, the deep gray matter "butterfly" is easily distinguished from the surrounding white matter in both the patients and healthy volunteers. Additionally, while obvious on the MTCSF images (arrow), lesions are less conspicuous on the MTR, T_1-weighted, and T_2-weighted measurements. Figure modified from Zackowski KM, et al, Brain 2009.

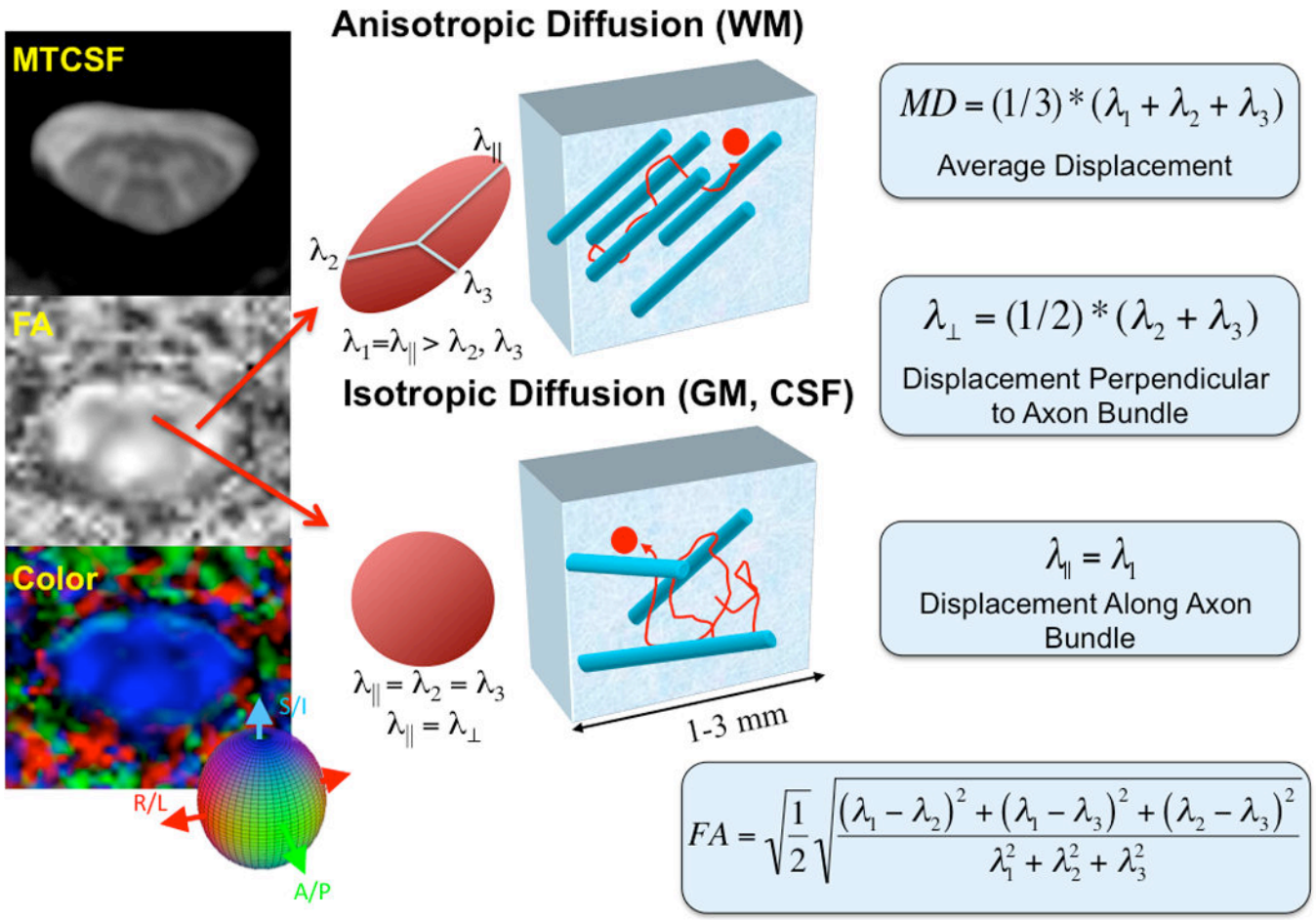

Figure 2.

Cartoon representation of conventional DTI methodology in the cervical spinal cord. In the left column, FA and colormaps of the cervical spinal cord are compared with an MTCSF image. The gray matter “butterfly” can be seen in both the FA and colormaps. In the middle panel, a visual description of tissue anisotropy for different regions of the spinal cord is presented. Note that in the anisotropic case (white matter), the principle Eigenvalue, $\lambda_{||}$ is greater than the orthogonal Eigenvalues, while in the isotropic case (gray matter), the three Eigenvalues are equal. At far right, metrics derived from DTI data are defined.

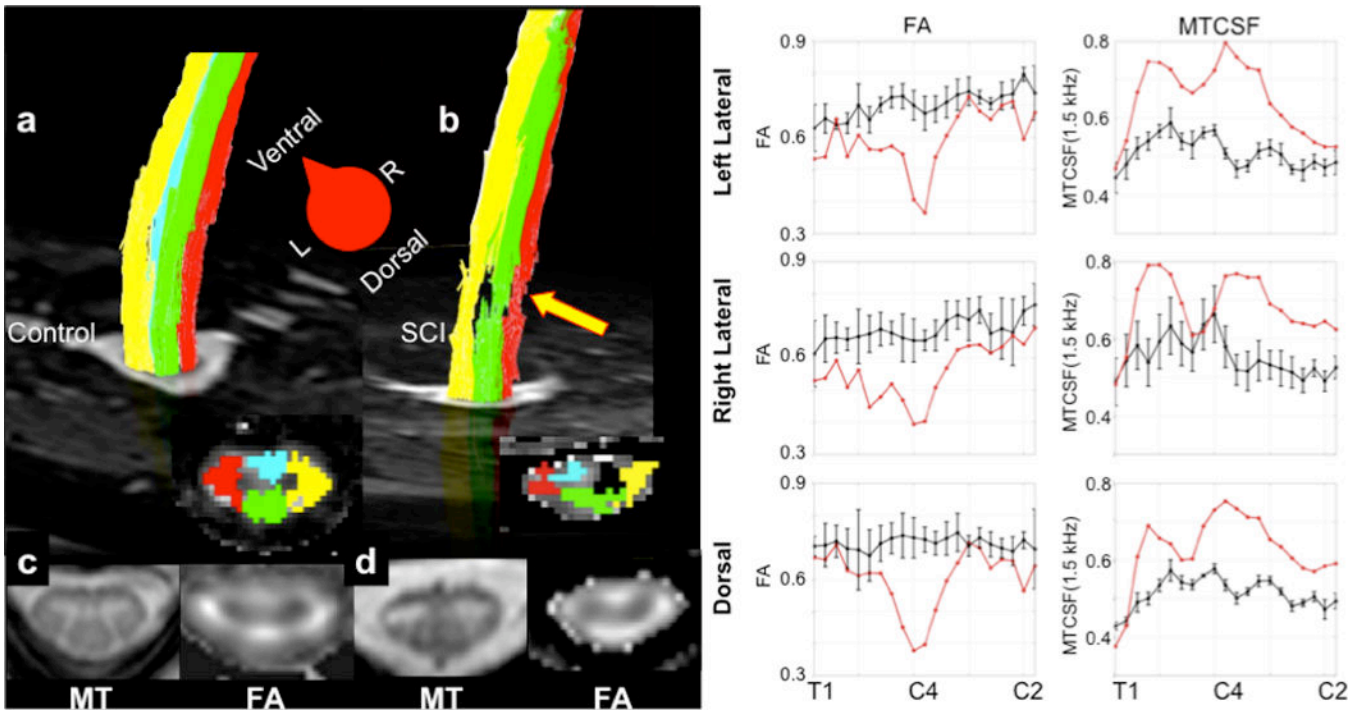

Figure 3.

Multi-modality imaging of the cervical spinal cord in a healthy volunteer and a patient with chronic spinal cord injury. a) and b) show reconstructed fiber pathways for the dorsal (green), lateral (right – red, and left – right). Note in the spinal cord injury case that fiber pathway damage is plainly visible (arrow). c) and d) show the MTCSF and FA maps at the level of the injury – C5 – in the spinal cord injury case and in the healthy volunteer. While the FA is high in the left lateral and dorsal columns, it shows a marked decrease in the right lateral column for the patient. The far right columns show tract-profiles for MTCSF and FA for the left lateral, right lateral, and dorsal columns for healthy volunteers (black) and the same patient presented in b). Note that FA decreases focally at the site of the lesion, but is close to normal rostral and caudal to the lesion. In contrast, the MTCSF values are elevated along the entire cervical cord. Figure modified from Smith SA, NMR in Biomedicine, 2010.

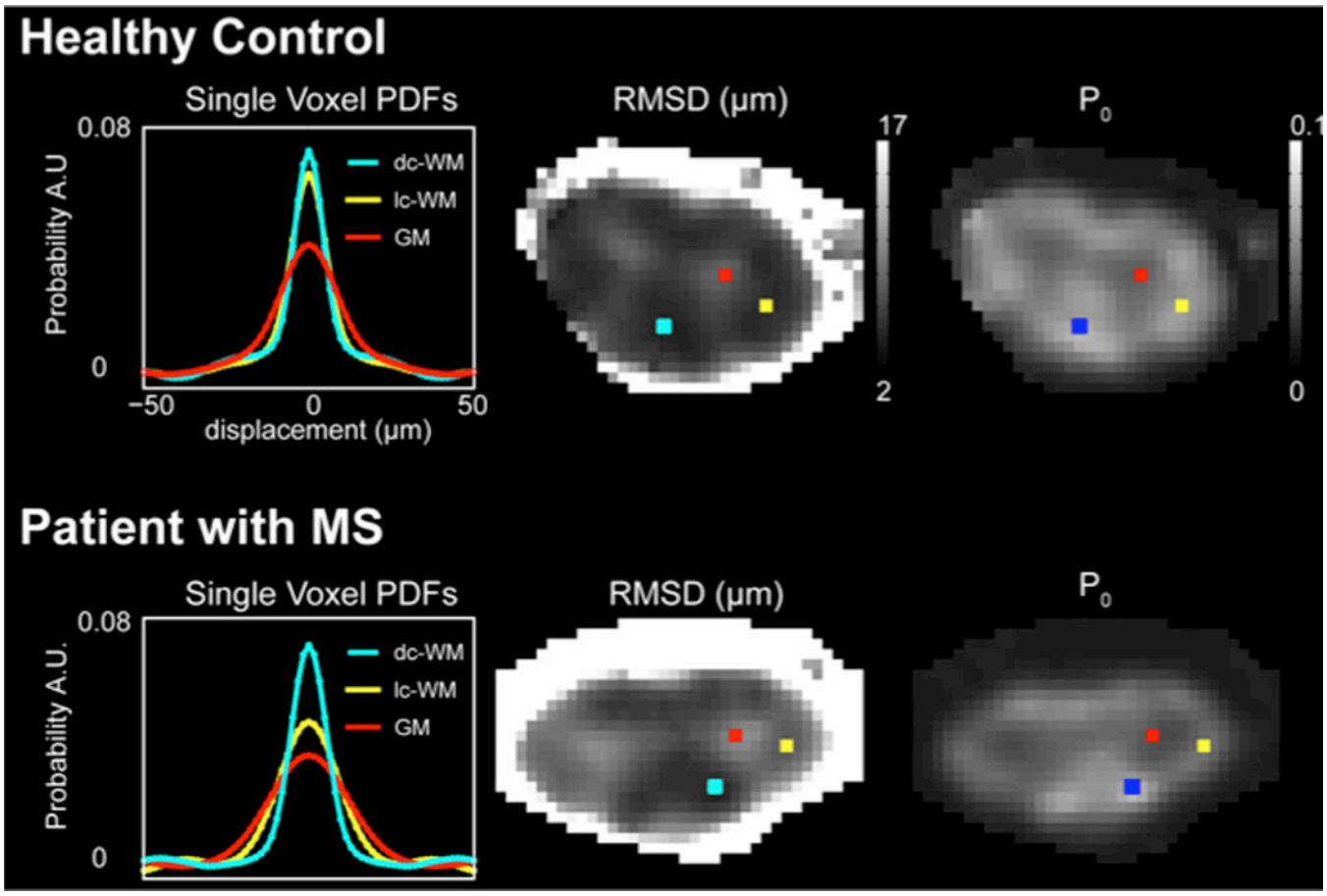

Figure 4.

Demonstration of q-space derived values of root mean square displacement (RMSD) and PDF height (P_0) in a healthy volunteer compared to a patient with MS. In the left panel, the q-space derived single voxel PDFs are shown for each of the voxels shown on the images. In normal white matter, it can be seen that a “healthy” PDF is tall and narrow (yellow and blue) while in gray matter (red) the PDF is low and broad. In the MS case with a prevalent lateral column lesion, the PDF for a voxel in the lesion (yellow) approximates the PDF for gray matter (red), while the uninjured column (dorsal column – blue) appears tall and narrow. For the derived RMSD and P0 maps, note that a high RMSD indicates a broader PDF while a high P0 indicates a tall PDF. Figure modified from Farrell JAD, et al, MRM 2008.

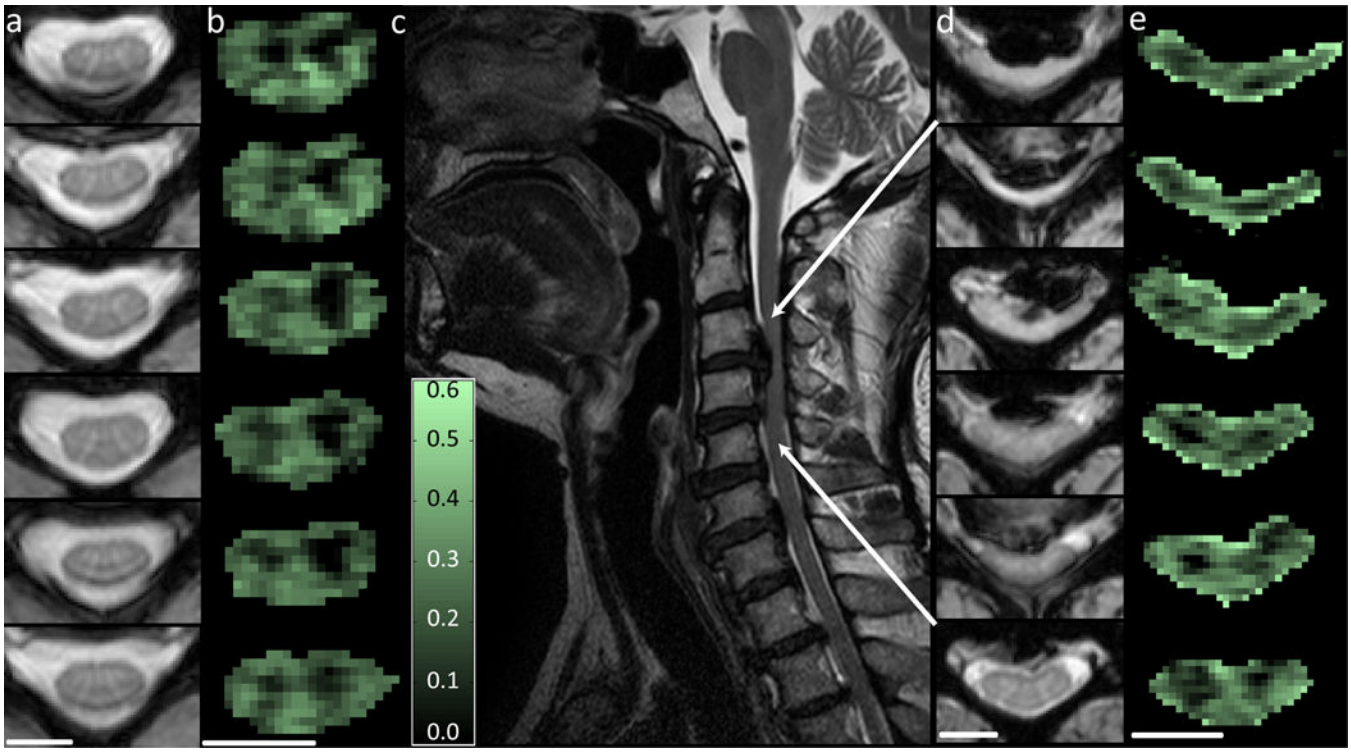

Figure 5.

Demonstration of the quantitative T_2 approach: myelin water fraction (MWF) images from a healthy control and a patient with cervical spondolysis. In the left panels, T_2-weighted and MWF maps of a healthy control are presented. The GM has a low MWF while the white matter appears brighter. In the center and right panels, a patient with cervical spondolysis is shown; the disc between C3–C4 is making contact with the spinal cord. The MWF maps at the site of spondolysis show a change in the myelin water fraction in each column, while, caudal to the lesion, the MWF maps appear normal. Images courtesy Dr. Alex MacKay and Dr. Erin Macmillan, University of British Columbia.

Table 1

Relative sensitivity to 1) myelin, 2) axonal, and 3) inflammatory pathology for each of the quantitative MRI methods described in the text. A "+" indicates that the method is sensitive to the selected pathology.

		Myelin	Axonal	Inflammation
Magnetization Transfer				
	MTR	+		
	MTCSF	+		+
	qMT	+		
Diffusion Tensor				
	Mean Diffusivity (MD)			+
	Fractional Anisotropy (FA)	+	+	
	Perpendicular Diffusivity ($\lambda_{\perp}$)	+		+
	Parallel Diffusivity ($\lambda_{\parallel}$)		+	+
q-Space				
	P0	+ (if across nerve)	+ (if along nerve)	
	RMSD	+ (if across nerve)	+ (if along nerve)	
Multi-Component T_2				
	Myelin Water Fraction (MWF)	+		
Spectroscopy				
	N-Acetyl Apartate (NAA)		+	
	Choline (Cho)	+		